Inorganic Chemistry

pubs.acs.org/IC
Article

Aqua–Chloro Complexes of Plutonyl in Hydrochloric Aqueous Solutions: Theoretical Study of Individual Contributions to XAS and UV–Vis Spectra

Gema Raposo-Hernández, Rafael R. Pappalardo, Andrea Melchior, and Enrique Sánchez Marcos*

Cite This: *Inorg. Chem.* 2026, 65, 19417–19428
Read Online

ABSTRACT: Plutonium speciation in high-salinity media remains difficult to characterize, yet it largely governs the geochemical fate of PuO_2^{2+} in marine environments. EXAFS and UV–vis measurements established that the evolution of specific spectral features correlates with the formation of successive aqua–chloro complexes. These signals represent a superposition of coexisting species in equilibrium, masking the individual contributions of each complex. In this work, we address this limitation with a combination of the nuclear ensemble approach (NEA) and high-level quantum-mechanical calculations, accounting for the relativistic Hamiltonian, spin–orbit coupling, and electron correlation, to isolate these overlapping contributions of the $[PuO_2(H_2O)_mCl_n]^{2-n}$ series and clarify the observed plutonyl speciation. The sensitivity of our methodology is quantified by comparing Wigner sampling against classical molecular dynamics (MD) trajectories. The results establish UV–vis spectroscopy as a high-resolution probe of the equatorial ligand field and provide a molecular basis for Pu(VI) speciation in saline environments.

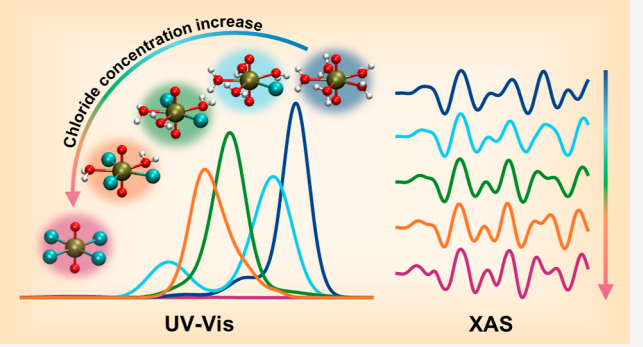

INTRODUCTION

The ocean serves as one of the primary geochemical sinks for anthropogenic pollutants, receiving both surface runoff and atmospheric deposition.[1−4] As global decarbonization efforts proceed, the nuclear industry represents a critical component of energy production; Europe alone operates over 100 reactors,[5] many of them located along the coast. This geographical proximity makes seawater a potential long-term reservoir for actinide contamination, necessitating a rigorous understanding of radionuclide interactions with seawater, a chemically complex medium dominated by high ionic strength and competing inorganic ligands. This is a critical concern regarding the bioaccumulation of heavy metals and radionuclides in marine food chains.[4,6,7]

Among actinides, plutonium is of particular concern because of its persistent radiotoxicity.[8] Its presence in marine environments comes from atmospheric tests of the 20th-century and point-source accidents, including the Chernobyl and Fukushima Daiichi disasters,[9−12] underscoring the need to understand actinide behavior in saline media. Elevated concentrations of competing anions, such as chloride, can drastically alter radionuclide speciation, solubility, and mobility.[13]

In aqueous solution, plutonium shows redox versatility, with oxidation states from III to VII. Pu(IV) is the predominant species in solution, but oxidizing or radiolytic environments stabilize higher oxidation states, making Pu(VI) relevant across both the nuclear fuel cycle and environmental systems.[14,15] In the PUREX process, plutonium is maintained in its actinyl form to facilitate its separation from minor actinides.[16] Parallel to this industrial relevance, the plutonyl cation, PuO_2^{2+}, exhibits a strong affinity for halide ligands in saline media, as does its uranyl UO_2^{2+} homologue.[17−22] However, chemical intuition derived from uranyl to plutonyl is limited. The electronic structure of Pu(VI), with two 5f electrons, is considerably more complex than that of U(VI). The $5f^2$ configuration generates a dense manifold of low-lying excited states with strong spin–orbit coupling and pronounced multireference character. A molecular-level description of the $[PuO_2(H_2O)_mCl_n]^{2-n}$ complexation connects microscopic electronic properties with the chemical behavior of high-valence plutonium in saline environments, even though Pu(VI) is a minor fraction of the total speciation in seawater.[23] Previous investigations of actinyl aqua and chloro complexes have combined spectroscopic measurements with theoretical

Received: June 2, 2026
Revised: July 28, 2026
Accepted: July 30, 2026
Published: August 9, 2026

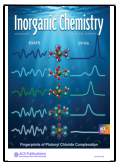

https://doi.org/10.1021/acs.inorgchem.6c02837
Inorg. Chem. 2026, 65, 19417–19428

modeling,[24−30] providing valuable structural and electronic insight while also revealing intrinsic limitations in species discrimination under equilibrium conditions.

X-ray absorption spectroscopies, in particular XANES and EXAFS, have been extensively applied to actinide systems to determine oxidation states, average coordination numbers, and metal−ligand bond distances in solution.[27,28,31] Complementary vibrational and electronic spectroscopies, such as Raman, UV−vis, or vis−NIR, provide additional sensitivity to molecular symmetry, ligand-field effects, and electronic transitions within the 5f manifold.[32,33] In principle, these techniques offer distinct spectral fingerprints for different coordination environments and ligand sets. However, in practice, the observed spectra frequently reflect a superposition of multiple species coexisting in equilibrium, particularly in high ligand concentration media, as is the case for concentrated chloride solutions.

As a result, although spectroscopy has firmly established the presence of chloro complexation in plutonyl systems, the precise nature and coordination of individual species remain subject to interpretation. A representative example is provided by the work of Runde et al.,[6] who investigated the plutonyl chloride system by monitoring the evolution of UV−vis and EXAFS spectra as a function of increasing chloride concentration. The formation of successive complexes is evidenced by the gradual spectral changes observed with increasing Cl^- concentration. At high chloride molarities, they observed a low-intensity absorption band, which they assigned to the tetrachloro complex, $[PuO_2Cl_4]^{2-}$. This assignment was further supported by Raman spectroscopy, where a vibrational mode (B_{2g}) appeared at frequencies consistent with the D_{4h} symmetry found in analogous actinyl−chloro complexes. Based on these observations, a decrease in the equatorial coordination number from five to four was proposed for the tetrachloro species. Nevertheless, the coordination environment of intermediate aqua−chloro complexes could not be unambiguously resolved. In particular, the intrinsic resolution limits of EXAFS when determining coordination numbers, typically associated with uncertainties of approximately ±1, preclude definitive structural assignments, leaving a gap that requires theoretical intervention to disentangle overlapping spectroscopic signatures.

Early DFT studies reproduced structural evolution and hydration of actinyl ions,[30,34,35] while more recent works show the importance of accounting for relativistic effects and electronic correlation in plutonium complexes.[36,37] In Pu(VI), the high density of excited states and significant spin−orbit coupling necessitate high-level multiconfigurational methods for chemical accuracy.

Despite the maturity of these computational methods, the theoretical reproduction of PuO_2^{2+} absorption spectra remains a formidable challenge due to the fundamental selection rules governing f−f transitions. As established by Matsika et al.,[38] since all low-lying electronic states for the isolated $5f^2$ actinyl ions possess the same parity (gerade), electric−dipole transitions are strictly Laporte-forbidden. The emergence of experimental intensity therefore relies on the breaking of inversion symmetry, either through the static effect of the equatorial ligand field or via vibronic coupling. Matsika et al.[38] demonstrated that the presence of chloride ligands in the equatorial plane facilitates the mixing of states with different parity, yet their models remained limited to specific coordination geometries. More recently, Danilo et al.[39] provided a rigorous description of the $[PuO_2(H_2O)_5]^{2+}$ electronic structure using CASPT2 and MRCI + DC methods, incorporating both the first hydration sphere and bulk solvent effects. However, a significant limitation persists in the literature: most theoretical studies rely on static optimized structures. In such high-symmetry configurations (e.g., D_{5h} or D_{4h}), the parity-breaking mechanisms are insufficiently captured, leading to calculated oscillator strengths that are either vanishingly small or identically zero. As a result, while transition energies can be predicted with high precision, direct simulation of experimental spectral bands has not been fully realized. This challenge is further highlighted by the recent findings of Neill et al.,[21] who demonstrated through a combined experimental and theoretical approach that equatorial halide ligands induce a significant electronic reorganization via an energy-match driven mechanism and a "pushing from below" effect on the frontier orbitals. Such perturbations suggest that the formation of successive plutonyl−chloro complexes should lead to substantial modifications in the electronic structure, potentially affecting both the transition energies and the intensities of the spectral signals. However, as these effects are inherently coupled to the local symmetry of the complex, their accurate reproduction in simulated spectra requires a methodology that moves beyond the static equilibrium approximation.

Since f−f transitions are formally Laporte-forbidden in centrosymmetric geometries, their nonzero intensity in solution arises from the symmetry-breaking distortions of the coordination environment. Static calculations from a single optimized structure cannot capture this effect, so we employ a nuclear ensemble approach based on Wigner sampling, which has proven effective for the absorption spectra of heavy-metal aqua ions and complex ligand environments.[40−44] High-level quantum mechanical (QM) calculations are performed over a representative distribution of geometries, generating ensemble-averaged spectra for the $[PuO_2(H_2O)_mCl_n]^{2-n}$ series. This enables a direct simulation of the absorption bands for each individual complex, separating their contributions to disentangle the complex speciation of plutonium in chloride-rich media.

METHODOLOGY

QM Calculations

Optimizations and frequency calculations were needed for Wigner sampling at room temperature (300 K). They were done by means of the second-order Møller−Plesset Perturbation Theory (MP2). The basis sets used are SD(60,MWB)/DEF-TZVP[45−47] for Pu and aug-cc-pVTZ[48] for Cl, O, and H.[48,49] Solvation effects beyond the first coordination shell were accounted for using the CPCM solvation model.[50]

To construct the electronic spectrum, we adopted a strategy similar to that employed in previous works, where aqua complexes of Ce^{3+} and U^{4+} were investigated.[40,41] This involved the systematic computation of the electronic structure for the plutonyl ion in its pentaaqua form, $[PuO_2(H_2O)_5]^{2+}$, and its subsequent series of aqua−chloro complexes, $[PuO_2(H_2O)_mCl_n]^{2-n}$ (where (m, n) = (4,1), (3,2), (2,3), and (0,4)).

The ground- and excited-state wave functions were derived from state-average Complete Active Space Self-Consistent Field (CASSCF)[51−53] calculations, including two electrons distributed over the seven 5f orbitals, resulting in 21 triplet

https://doi.org/10.1021/acs.inorgchem.6c02837
Inorg. Chem. 2026, 65, 19417−19428

states and 28 singlet states. Dynamical correlation was incorporated using the N-electron valence state perturbation theory NEVPT2,[54−56] keeping the 1s oxygen atomic orbitals and all plutonium core orbitals below the 5d orbitals frozen. In addition, CASPT2[57−59] calculations were performed using the ionization potential electron affinity (IPEA)-corrected zeroth-order Hamiltonian[60] while keeping the same frozen core definition as described above. An imaginary shift of $0.25E_h$ was used to avoid intruder states.

The relativistic Hamiltonian employed is the Exact Two-Component Hamiltonian (X2C), which provides an accurate description of the relativistic effects on actinoids.[61−65] This method utilizes the X2C Hamiltonian with the X2C-TZVPall basis sets[66,67] for O and H and the cc-pVQZ-X2C basis set[68] for Pu. Several authors[69,70] have performed calculations of properties depending on relativistic effects and spin−orbit couplings on actinides. They used specific basis sets of triple-ζ quality (cc-pVTZ-X2C[69] and ANO basis sets truncated to the triple-ζ level[70]). They have shown good results when compared to the experimental data. The inclusion of spin−orbit (SO) coupling was done using mean-field approximation (SOMF)[71] combined with the resolution of the identity (RI-SOMF(1X)). An example of an input file is included in the Supporting Information (SI). All calculations were conducted using the ORCA 6.1 software.[72,73]

Statistical Sampling: Molecular Dynamics and Wigner Distribution

In the context of PuO_2^{2+} UV−vis spectroscopy, the relevant excited states correspond to Laporte-forbidden f−f transitions. It is essential to sample distorted molecular configurations to capture the intensity that arises from symmetry breaking and ligand-field splitting. Two complementary sampling methods were used to generate or to extract statistically significant sets of geometry for spectrum generation: Wigner sampling and classical molecular dynamics (MD) simulations. Classical MD simulations are a valuable technique for statistical sampling, especially when the force field (FF) parameters are derived from high-level quantum mechanical (QM) calculations. However, this approach presents some limitations, including the elaborated FF parametrization and the requirement for system-specific parameter sets, which restricts its transferability to the successive chloro species. Our group developed a set of FFs for describing actinyl AnO_2^{2+} cations, with An = U(VI), Np(V,VI), Pu(VI), and Am(VI), in water.[74−76] A series of snapshots were extracted from a 5 ns simulation of a cubic box containing the actinoid and 1495 TIP4P water molecules. The time step of 1 fs was selected, and the average temperature and pressure were kept constant at 300 K and 1 atm using the Nosè−Hoover barostat. Additional methodological details of the MD simulation can be found in refs[74−76].

Another widely used technique for generating distorted molecular geometries is Wigner sampling,[77−79] which creates an ensemble of structures based on the harmonic normal vibrational modes obtained at the potential energy surface (PES) minimum of the target system.[80] This method circumvents the need for classical FFs or computationally demanding ab initio molecular dynamics; it relies on the harmonic description, which can be less accurate for systems with low-frequency modes or high conformational flexibility. Wigner sampling is well-suited for studying the complexation and speciation of heavy metals in aqueous environments, where metal−ligand interactions are predominantly ionic and the degree of anharmonicity is minimal. In this work, Wigner distributions were generated at 300 K based on the optimized structures and harmonic vibrational frequencies, using the *wigner.py* utility from the SHARC package.[81] The frequencies below 250 cm^{-1} for the aqua ion and 200 cm^{-1} for the aqua chloro species were discarded to avoid artificial O−H displacements originating from the description of torsional modes.[82,83]

Methodological Approach to Calculating Average EXAFS, XANES, and UV−Vis

The average EXAFS spectra were computed from 500 individual spectra obtained from sampled configurations. Pu L_{III}-edge k^3-weighted spectra were computed including multiple scattering (MS) up to four legs and a maximum path length of 6 Å. Details regarding the generation of EXAFS using self-consistent calculation of the wave function, with the Hedin−Lundqvist exchange correlation functional, can be found in prior works.[84−86] An example of the FEFF input file to compute the EXAFS signal is provided in the SI.

Since the absolute intensity scale of the experimental EXAFS data was not explicitly provided in the source literature,[21] the experimental signal was scaled to match the amplitude of the theoretical spectrum calculated with an amplitude reduction factor (S_0^2) of 1.0. The energy correction of the threshold, ΔE_0, is fixed to −2.0 eV to make the first oscillation of the theoretical spectra match the first oscillation of the aqua ion experimental spectrum. For the calculations of XANES spectra, the number of individual spectra averaged was reduced to 100 sampled configurations, as this part of the XAS spectrum is less sensitive to geometrical fluctuations. In the SCF computations, the Hedin−Lundqvist exchange correlation functional provided an ideal balance between the intensity of the white line and subsequent resonances. No shift in energy was applied to the theoretical spectra to match the experimental edge position. An input file for the XANES computation is also given in the SI. EXAFS and XANES spectra have been simulated using the structural information and the theoretical scattering phases and amplitude functions computed by the ab initio FEFF code (v.10.0.0).[87,88]

The average UV−vis spectra were reconstructed from 100 individual spectra using the Gaussian Mixture Model-Nuclear Ensemble Approach (GMM-NEA).[89]

RESULTS

Structural Characterization

To correlate the structural evolution of the plutonyl core with its spectral response in saline environments, we first characterized the variations in the equatorial coordination sphere induced by chloride complexation. Tables 1 and 2 benchmark the MP2-optimized geometries of the $[PuO_2(H_2O)_5]^{2+}$ aqua ion and its chloro derivatives, $[PuO_2(H_2O)_mCl_n]^{2-n}$, against the available experimental and theoretical literature, reflecting the spread in reported coordination environments. A representation of the optimized structures is included in Figure S1 of the SI.

For the pentaaqua species, the calculated axial Pu−O_{yl} distance (1.728Å) is slightly shorter than the experimental range of 1.74 Å to 1.76 Å determined by EXAFS and XANES.[6,21,91] This underestimation is typical of the MP2 performance in actinyl systems, arising from the treatment of subvalence correlation. Nevertheless, the equatorial Pu−OH_2 bond length of 2.397Å aligns with the lower bound of

https://doi.org/10.1021/acs.inorgchem.6c02837
Inorg. Chem. 2026, 65, 19417−19428

Table 1. Summary of Pu−O_{yl} and Pu−OH_2 Average Distances and Coordination Numbers (CNs) Obtained from Experiments and Geometry Optimizations for $[PuO_2(H_2O)n]^{2+}$ Aqua Ions

method (solvation)	R_{Pu-Oyl} (Å)	R_{Pu-OH_2}(Å)	CN	ref
MP2 (CPCM)	1.728	2.397	5	this work
MD (Explicit)	1.71	2.45	5	26
B3LYP	1.71	2.46	5	26
NEVPT2	1.76	2.43	5	26
B3PW91 (CPCM)	1.70	2.42	5	90
BP86 (Microsolvated)	1.76	2.40−2.41	5	34
PBE(PCM)	1.748	2.441	5	30
B3LYP (PCM)	1.718	2.435	5	30
EXAFS	1.74	2.42	4.4	91
EXAFS	1.74	2.45	-	6
EXAFS	1.76	2.41	5.3	21
XANES	1.75	2.41	4.5	31

experimental values of 2.41 Å to 2.45 Å, providing a consistent structural baseline for the subsequent substitution series.

Substitution of equatorial water by chloride ligands expands the coordination shell. The Pu−OH_2 distance increases to 2.502 Å in the tetrachloride complex, while Pu−Cl distances evolve from 2.644 Å to 2.728 Å. These trends correlate with the results reported by Neill et al.,[21] Conradson et al.,[31] and Runde et al.,[6] where Pu−Cl distances within the 2.69 Å to 2.75 Å range were observed at high salinity. As the number of chloride ligands (n) increases in the $[PuO_2(H_2O)_mCl_n]^{2-n}$ series, we observe a subtle but consistent elongation of the Pu−O_{yl} bond, which reaches 1.741 Å in the tetrachloro complex. This trend comes from the stronger equatorial donation from the anionic chloride ligands compared to the neutral water molecules; this higher electron density on the Pu center slightly weakens the axial Pu−O_{yl} interaction. The equatorial Pu−Cl bond lengths exhibit an expansion as the coordination sphere becomes more crowded. In the intermediate species, where the total coordination number (CN) remains 5, the Pu−Cl distances range from 2.644 Å to 2.728 Å. This expansion is driven by both the larger ionic radius of Cl^- and the increasing steric repulsion between ligands in the equatorial plane.

The most significant structural transition occurs with the formation of the tetrachloro species, $[PuO_2Cl_4]^{2-}$. While the hydrated chloro complexes favor a pentacoordinated equatorial plane, the anhydrous tetrachloro complex has a CN of 4, with a D_{4h} symmetry. The decrease in coordination number with anionic ligands in the first coordination shell has been reported in the evolution of the CN of Po^{4+} hydrates when water molecules are replaced by hydroxyl anions.[92,93] The change in coordination number is accompanied by a notable contraction of the Pu−Cl bonds to 2.645Å as the loss of the fifth equatorial ligand (water) relieves the steric repulsion. The structural reorganization from 5 to 4 ligands provides a molecular basis for the Raman B_{2g} vibrational mode identified by Runde et al.[6] at high chloride concentrations. This transition from D_{5h} to D_{4h} not only dictates the vibrational modes of the complex but also changes the symmetry-allowed transitions governing the electronic absorption spectra, as will be discussed in the following sections.

EXAFS

To validate the MP2 Wigner sampled ensemble, the theoretical k^3-weighted EXAFS spectrum was compared with experimental data[21] for the $[PuO_2(H_2O)_5]^{2+}$ aqua ion (Figure S2). The computed signal reproduces the experimental phase and amplitude, particularly within the characteristic 6 $Å^{-1}$ to 9 $Å^{-1}$ k region. The good agreement in the oscillation frequency confirms that both the Pu−O_{yl} and Pu−OH_2 bond lengths are accurately captured by the sampling approach, providing a strong foundation for the subsequent analysis of the chloro-substituted series.

The evolution of the experimental EXAFS spectra[21] as a function of chloride concentration (Figure 1) is characterized by the changes in the 7 $Å^{-1}$ to 9 $Å^{-1}$ region. In the aqua ion case, $[PuO_2(H_2O)_5]^{2+}$, the spectral profile in this range is governed by the interference between the plutonyl oxygen atoms Pu−O_{yl} and the water ligands Pu−OH_2 paths, as shown in Figure S3 of the SI. As chloride ligands substitute water molecules, the expansion of the equatorial shell, shown in Table 2, modulates the phase and position of the single-scattering (SS) signals, directly affecting the k ∼7 $Å^{-1}$

Table 2. Summary of Pu−O_{yl}, Pu−OH_2, and Pu−Cl Average Distances Obtained from Experiments and Geometry Optimizations for $[PuO_2(H_2O)_mCl_n]^{2-n}$ Aqua−Chloro Complexes

method (solvation)	R_{Pu-Oyl} (Å)	R_{Pu-OH_2}(Å)	CN_{OH2}	R_{Pu-Cl} (Å)	CN_{Cl}	refs
MP2 (CPCM)	1.732	2.421	4	2.644	1	this work
MP2 (CPCM)	1.735	2.451	3	2.662	2 (trans)	this work
MP2 (CPCM)	1.735	2.456	3	2.658	2 (cis)	this work
MP2 (CPCM)	1.737	2.477	2	2.688	3 (trans)	this work
MP2 (CPCM)	1.737	2.494	2	2.691	3 (cis)	this work
MP2 (CPCM)	1.739	2.502	1	2.728	4	this work
MP2 (CPCM)	1.741	-	0	2.645	4	this work
B3PW91 (CPCM)	1.77	2.59	4	2.98	1	90
B3PW91 (CPCM)	1.72	2.50	3	2.66	2	90
BP86 (Microsolvated)	1.79	-	0	2.67−2.68	4	34
EXAFS ([Cl^-] 2M)	1.75	2.43	4.5	2.69	0.3	21
XANES ([Cl^-] 4M)	1.75	2.43	2.7	2.75	1.3	31
EXAFS ([Cl^-] 5M)	1.75	2.43	-	2.75	-	6
EXAFS ([Cl^-] 6M)	1.75	2.42	3.6	2.73	1.3	21
XANES ([Cl^-] 16M)	1.75	2.49	2.6	2.70	2.4	31
EXAFS ([Cl^-] 16M)	1.75	2.49	-	2.70	-	6

https://doi.org/10.1021/acs.inorgchem.6c02837
Inorg. Chem. 2026, 65, 19417−19428

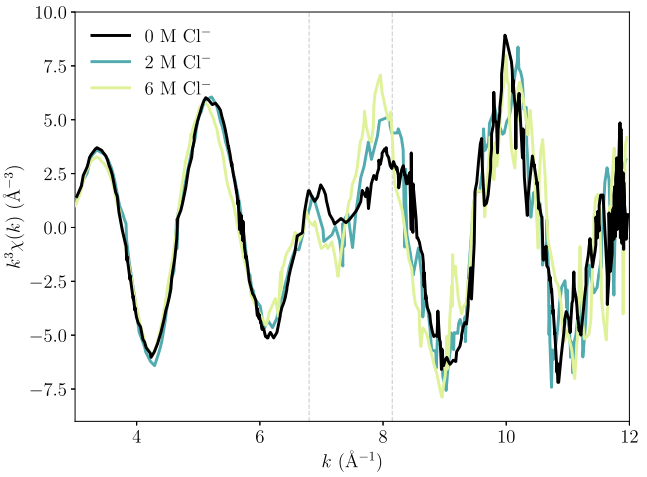

Figure 1. Evolution of experimental EXAFS spectra as a function of chloride concentration adapted from Neill et al.,[21] Copyright 2025 American Chemical Society, ($[PuO_2^{2+}]$ = 5 mM). Vertical lines at 6.8 Å^{-1} and 8.15 Å^{-1} are included as visual references.

shoulder, as shown in the overall spectral trends observed in Figure 2.

Analysis of the individual SS contributions for $[PuO_2(H_2O)_3Cl_2]$, plotted in Figure 3, reveals that the Pu−Cl path exhibits a scattering frequency similar to that of the Pu−OH_2 path. In the $k \sim 8$Å^{-1} region, all three primary contributors (Pu−O_{yl}, Pu−OH_2, and Pu−Cl) undergo constructive interference, as evidenced by the alignment of their oscillatory maxima. The substitution of water by chloride introduces a heavier scatterer that increases the amplitude of the total oscillation, affecting the oscillation intensity at k ∼ 8 Å^{-1}. At the same time, this substitution induces an evolution of the coordination shell distances. The Pu−Cl bonds, longer than their Pu−OH_2 counterparts, reach a maximum elongation in the trichloro complex before contracting in the tetrachloro species as the total coordination number (CN) shifts from 5 to 4. As shown across the full series (Figure 4), these combined effects produce a progressive enhancement of the feature at k ∼ 8 Å^{-1} and the restructuring of the k ∼ 7 Å^{-1} feature, which are the structural fingerprint of the equatorial reorganization induced by chloride coordination.

XANES

To evaluate the Pu(VI) speciation in chloride media, we analyzed the evolution of the XANES spectra as a complementary diagnostic tool. As shown in Figure 5, the experimental L_{III}-edge spectra are somewhat insensitive to increasing chloride concentration. The position of the absorption edge and the white-line intensity show only minor fluctuations, indicating that the Pu(VI) oxidation state and the *trans*-dioxo core symmetry are strictly preserved throughout the substitution series.

However, a closer examination of the experimental series reveals some sensitivity to the chloride concentration. Notably, the spectral variation observed when increasing the salinity from 1.3 to 2.4 M Cl^- (green vs orange lines) is more pronounced than the change recorded between the aqua ion (0 M) (black vs green lines) and the 1.3 M condition. This observation suggests that the transition toward higher-order chloro complexes (such as the di- or trichloro species) induces a more significant perturbation of the plutonium electronic density than the initial monosubstitution.

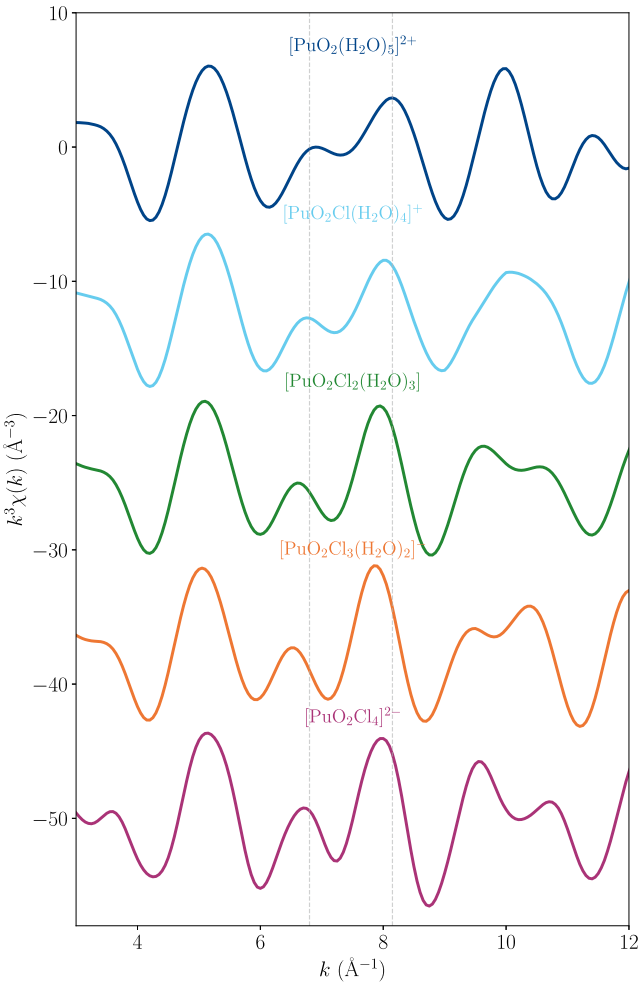

Figure 2. Theoretical EXAFS spectra of the $[PuO_2(H_2O)_mCl_n]^{2-n}$ series. Vertical lines at 6.8 Å^{-1} and 8.15 Å^{-1} are included as visual references. The $[PuO_2(H_2O)_3Cl_2]$ and $[PuO_2(H_2O)_2Cl_3]^-$ spectra correspond to the *trans* isomer; the results with the *cis* isomer are equivalent.

The theoretical XANES spectra, computed for the $[PuO_2(H_2O)_mCl_n]^{2-n}$ series (Figure 6), follow the same trend observed in the experimental spectra and reproduce the shoulder on the high-energy side of the white line (18,085 eV), which is characteristic of the multiple scattering (MS) processes within the Pu−O_{yl} bonds.[94]

Neill et al.[21] have recently recorded the Pu M4-edge of the plutonyl aqueous complex at 0 and 6 M of hydrochloric acid. Figures S4 and S5 in SI show a comparison of the experimental spectra with the simulated ones for the plutonyl pentahydrate and one of the aqua−chloro complexes. The chloride concentration increase is qualitatively reproduced in both the edge position and the shift of the second maximum at about 3977 eV.

UV−Vis

For the characterization of the $5f^2$ electronic manifold in the plutonyl ion, we employed a CASSCF(2,7) reference space comprising the two valence electrons distributed among the seven 5f orbitals. Two perturbative schemes were considered: NEVPT2 and CASPT2. To assess the consistency of our approximation, we compare the results to the experimental transitions reported by Edelstein[95] for the case of the plutonyl

https://doi.org/10.1021/acs.inorgchem.6c02837
Inorg. Chem. 2026, 65, 19417−19428

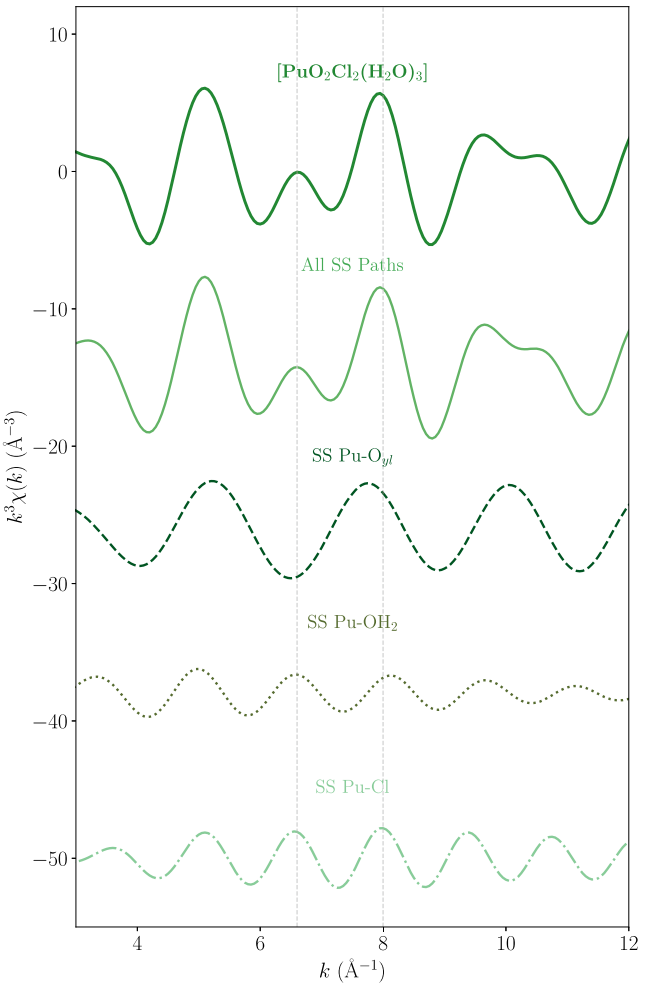

Figure 3. Theoretical EXAFS spectrum of $[PuO_2(H_2O)_3Cl_2]$ and the contribution of single scattering paths. To aid in correlating spectral features with their specific single scattering (SS) origins, vertical markers are included at 6.6 $Å^{-1}$ and 8 $Å^{-1}$ as a visual reference.

aqua ion. To prevent the artificial splitting of degenerate states, vertical transitions were computed by using a D_{5h}-symmetrized structure for $[PuO_2(H_2O)_5]^{2+}$, allowing for a consistent assignment based on the irreducible representations of the point group.

The comparison in Table 3 shows that NEVPT2 and CASPT2 agree closely in the near-infrared (NIR) region, with a nonlinear divergence that emerges as the manifold progresses toward higher energies, with the NEVPT2 values being consistently higher than their CASPT2 counterparts. Both methods show a systematic blue shift relative to the experimental data. This overestimation is well-documented in the multireference treatment of actinyl systems[39] and reflects the inherent difficulty of second-order perturbation theory to fully recover the dynamic correlation between the 5f electrons and the 6s/6p subvalence shells. The 5d, 6s, and 6p subvalence shells were kept frozen during the perturbative step. Unfreezing these shells could partially recover core−valence correlation, but the standard cc-pVQZ-X2C basis set[68] is primarily optimized for valence correlation. Incorporating subvalence correlation without the corresponding core-consistent (CV) functions would not yield an improved description while significantly increasing the computational cost.

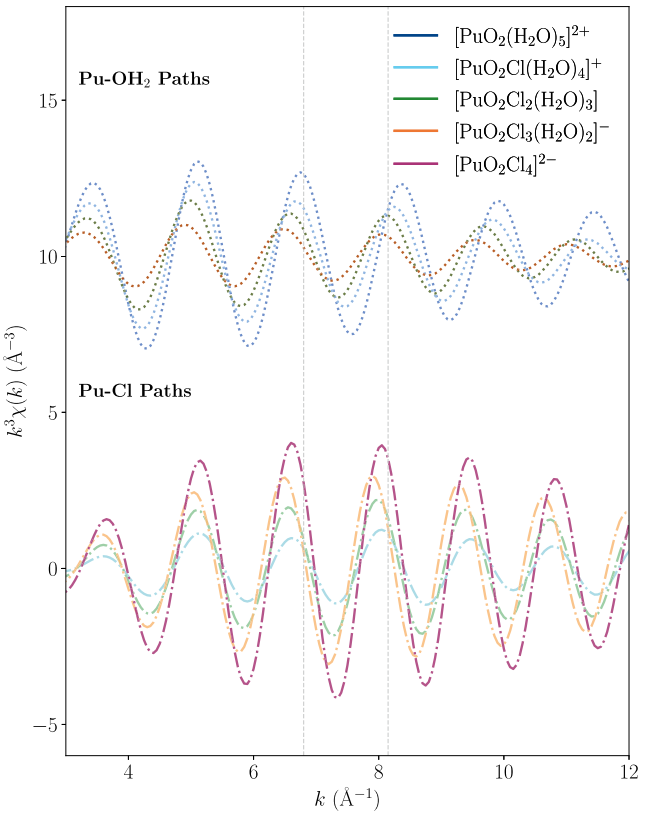

Figure 4. Theoretical EXAFS contributions of Pu−OH_2 and Pu−Cl single scattering paths. Consistent with previous figures, the vertical lines at 6.8 $Å^{-1}$ and 8.15 $Å^{-1}$ are visual references.

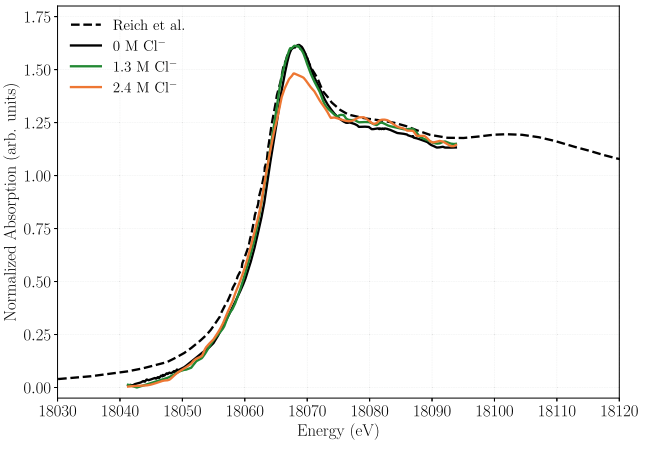

Figure 5. Evolution of experimental XANES spectra as a function of chloride concentration extracted from ref 31, Copyright 2004 American Chemical Society. The XANES spectrum of the aqua ion $[PuO_2(H_2O)_5]^{2+}$ from Reich et al.[91] is also included.

We applied uniform scaling factors (σ_{NEVPT2} = 0.873; σ_{CASPT2} = 0.893) to align our theoretical results with the position of the experimental Band F (12,045 cm^{-1}). This transition was chosen as the reference point due to its high intensity and its sensitivity to perturbations in the ligand sphere. Both NEVPT2 and CASPT2 yield comparable mean absolute errors (MAEs) (429 cm^{-1} to 433 cm^{-1}) once the systematic blue shift is corrected. This confirms that both schemes effectively recover the relative spacing of the $5f^2$ manifold. Nevertheless, NEVPT2 was adopted as the

https://doi.org/10.1021/acs.inorgchem.6c02837
Inorg. Chem. 2026, 65, 19417−19428

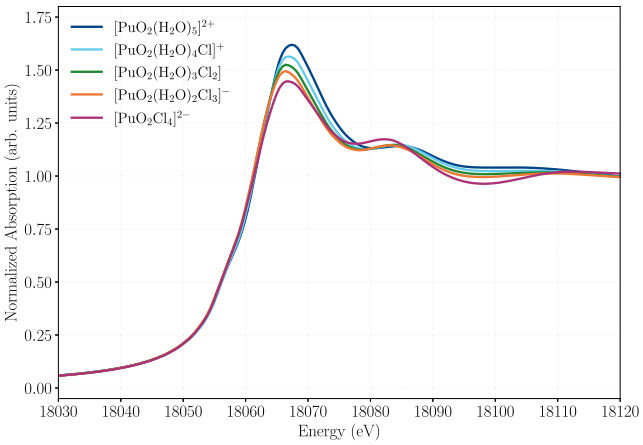

Figure 6. Theoretical XANES spectra of the $[PuO_2(H_2O)_mCl_n]^{2-n}$ series.

computational method for our subsequent analysis, since it offers a parameter-free formulation that avoids the need for empirical corrections, like the IPEA shift, which is often required in CASPT2 to prevent intruder state problems. NEVPT2 is also computationally more efficient with the large cc-pVQZ-X2C basis set, allowing the extension of the methodology to the sampled geometries. When the methodology was extended to the GMM-NEA convoluted spectra, the NEVPT2 scaling factor was slightly refined to 0.863 to match the experimental Band F position. Reproducing the position of Band F in the aqua ion ensures that the relative red-shifts observed upon chloride substitution are consistently captured.

The methodology relies on both configurational sampling and electronic structure methods. This is illustrated in the comparison of Wigner sampling and MD trajectories for the $[PuO_2(H_2O)_5]^{2+}$ aqua ion (Figure S7 of the SI), where the MD-derived spectrum is substantially broader than the sharp experimental band F that the Wigner approach reproduces. The observed discrepancies demonstrate the sensitivity of our spectroscopic model to differences in structural distribution.

The origin of the observed spectral differences is a direct consequence of the distance distributions shown in Figure S8 of the SI. MD trajectories sample a wider range of Pu−O equatorial distances, including a "tail" of distorted configurations that do not appear in the Wigner distribution. This arises from the potential energy surface (PES) used to parametrize the MD force field. Since this PES was constructed

Table 3. Comparison of Experimental and Calculated Electronic Transitions (cm^{-1}) for the $[PuO_2(H_2O)_5]^{2+}$ Aqua Ion[d]

Edelstein et al.[a]		Edelstein et al.[a]		Danilo et al.[b]		This Work[c]			
State ($D_{\infty h}$)	Band	Exp	Calc	State (Ω)	Calc. (PCM)	NEVPT2	CASPT2	Scaled NEVPT2 (σ = 0.873)	Scaled CASPT2 (σ = 0.893)
E_{4g}		0	0.8	4_g	0	0	0	0	0
A_{1g}	–	–	2143	0_g^+	2657	1828	2155	1596	1924
E_{1g}	–	–	3823	1_g	4914–4930	4371	4474	3816	3995
E_{5g}	A	7385	7277	5_g	7751–7821	7645	7649	6674	6831
E_{1g}	B	10187	10228	0_g^-	11643	11942	11538	10425	10304
A_{1g}	C	10442–10526	10427	1_g	11528–11543	11007	11024	9609	9844
A_{2g}	D	10706	10593	0_g^+	12392	12265	11947	10708	10668
E_{2g}	**F**	**12045**	**12129**	$\mathbf{2_g}$	**13656**	**13805**	**13494**	**12052**	**12050**
E_{6g}	G	12643	12943	6_g	14222–14228	13951	13867	12179	12383
-	H	12866	–	–	–	–	–	–	–
E_{4g}	–	–	13863	–	–	–	–	–	–
A_{1g}	–	–	15684	–	–	15481	15506	13515	13847
–	I	15458	–	0_g^+	18442	17941	17990	15663	16065
E_{3g}	J	16055	16128	4_g	18643–18685	–	–	–	–
–	K	16880	–	–	–	–	–	–	–
E_{2g}	L	17799	17836	1_g	20810–20834	21097	20696	18418	18483
E_{1g}	–	–	18260	–	–	–	–	–	–
A_{1g}	N	19111	19098	–	–	22196	21797	19377	19464
E_{5g}	O	19811	19827	0_g^+	22101	24325	24533	21235	21908
E_{2g}	–	–	20137	–	–	26403	24610	23049	21977
E_{1g}	P	21239	21223	5_g	24892–24918	26871	25215	23458	22517
E_{4g}	Q	21828	21736	1_g	26387–26389	27496	26125	24004	23330
E_{1g}	–	–	22556	6_g	29202–29300	29249	27980	25534	24986
–	–	–	–	0_g^+	36612	30191	29717	26356	26537
Mean Absolute Error						**2453**	**2269**	**429**	**433**

[a]Crystal field analysis and experimental assignment from Edelstein.[95] [b]CASPT2/SO-RASSI results with implicit solvation from Danilo et al.[39] [c]This work. Calculated VEE using a CASSCF(2,7) reference. Scaled values are obtained by multiplying the raw energies by σ = 0.873 (NEVPT2) and σ = 0.893 (CASPT2) to match the energy of Band F. [d]Theoretical values from this work are presented both as raw VEEs and after applying a uniform scaling factor (σ).

https://doi.org/10.1021/acs.inorgchem.6c02837
Inorg. Chem. 2026, 65, 19417−19428

using the B3LYP functional, it struggles to fully describe the complex electron correlation effects inherent to the plutonyl center, which has been demonstrated to be crucial for a proper description of the structure and dynamics of actinides in solution.[26,86,96] The treatment of water molecules is fundamentally different in both methods; whereas Wigner sampling captures the quantum vibrational ground state from the MP2 method, the MD simulation employs a rigid water model. The combination of these structural differences accounts for the enhanced bandwidth and the band displacement observed for Band F. The UV−vis spectrum can thus distinguish between these two sampling methods. These results confirm that Wigner sampling provides a reliable baseline for this system and justify its use to track the subtle spectral evolution with chloride complexation.

Given the agreement obtained with the NEVPT2 protocol for the aqua ion, we extended this scheme to the study of the $[PuO_2(H_2O)_mCl_n]^{2-n}$ series. Our goal is to evaluate the ability of the methodology to reproduce the systematic red-shift observed experimentally as the chloride concentration increases. To characterize the speciation of PuO_2^{2+} in chloride media, the evolution of the experimental spectra was reconstructed by integrating multiple sources from the literature. The reference spectrum for the aqua ion was obtained by digitizing high-resolution data from Edelstein,[95] particularly in the lower-intensity spectral regions. This digitized baseline was combined with a Gaussian function centered at the main absorption band, calibrated to a molar absorptivity of 550 M^{-1} cm^{-1} as established by Cohen[97] and Gaunt et al.[32] (see Figure S6 in the SI for the complete representation). The experimental absorption spectra for the aqua−chloro complexes were derived from the data reported by Runde et al.[6] To account for the absence of absolute intensity units in the original data set, the molar absorptivity of the 1.5 M Cl^- spectrum was set to 145 M^{-1} cm^{-1}, following the experimental values established by Lee et al.[98] for the complex species at 1 M HCl. Adopting this specific intensity as a reference while strictly maintaining the internal relative proportions of the Runde et al.[6] series, a consistent molar absorptivity scale was established for all chloride concentrations. This approach ensures that the systematic spectral evolution observed as a function of the ligand concentration remains comparable across different studies.

In Figure 7, the spectral evolution of Band F shows that increasing chloride concentration does not result in a simple shift of a single peak. Instead, the spectrum undergoes a dramatic transformation characterized by the sequential replacement of distinct bands. The narrow, dominant band of the aqua ion at 12,045 cm^{-1} (0 M Cl^-) decreases in intensity, while new features grow in at lower energies. For intermediate chloride concentrations (1.5 to 5 M), a complex set of peaks is observed in the range of 11,800 cm^{-1} to 12,045 cm^{-1}. At higher concentrations (7 to 16 M), these intermediate features merge and shift further, consolidating into a single, broader band envelope with its maximum at approximately 11,800 cm^{-1} at the highest salinity condition. These complex spectral changes, arising from highly sensitive f−f transitions, reflect the specific perturbation of the PuO_2^{2+} equatorial ligand field as water molecules are progressively replaced by chloride ions. The fact that individual experimental spectra for pure intermediate species are unavailable, as they exist solely in equilibrium in solution, prevents a direct comparison with computed spectra of isolated complexes.

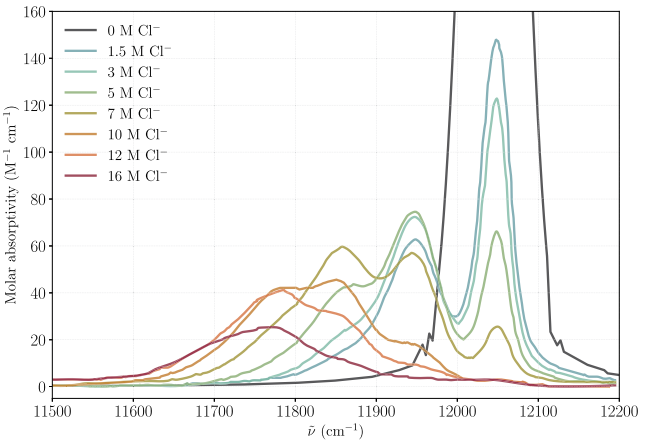

Figure 7. Evolution of the experimental spectra as a function of chloride concentration. The aqua ion spectrum (0 M Cl^-, black line) was adapted from Edelstein,[95] Copyright 2025 American Chemical Society, while the remaining spectra were adapted with permission from the work of Runde et al.,[22] Copyright 1999 Elsevier.

Comparing the experimental series with the theoretical predictions in Figure 8 reveals a correlation with spectral shifts

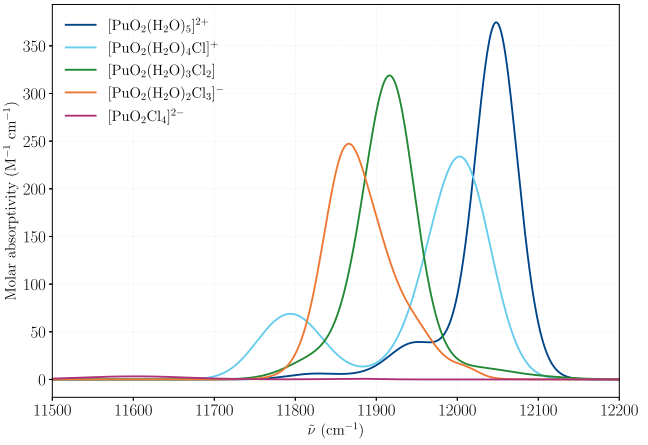

Figure 8. Evolution of the theoretical spectra with the increase of chloride anions in the first coordination shell of the PuO_2^{2+} cation. The spectra of $[PuO_2(H_2O)_3Cl_2]$ and $[PuO_2(H_2O)_2Cl_3]^-$ are the result of weighted averages based on the relative populations of their isomers, 85/15 and 95/5, respectively.

and specific coordination environments. For the cases of the dichloro and trichloro derivatives, two different isomers are possible. The calculated spectra represent the intermediate $[PuO_2(H_2O)_3Cl_2]$ and $[PuO_2(H_2O)_2Cl_3]^-$ species as statistically weighted averages of their isomers (using 85/15 and 95/5 ratios, respectively, shown in Figure S9), based on the Boltzmann distribution derived from their relative energies. The NEVPT2 calculations reproduce the experimental trend, with a systematic red-shift as each water molecule is substituted by chloride ligands in the equatorial plane. The main band for the aqua ion centered at 12,050 cm^{-1} shifts to 12,000 cm^{-1} for the monochloro derivative, to 11,900 cm^{-1} for the averaged dichloro complex, to 11,850 cm^{-1} for the averaged trichloro complex, and to 11,600 cm^{-1} for the tetrachloro derivative, but the absorptivity is ∼3 M^{-1} cm^{-1}, almost 100 times smaller than the other derivatives.

https://doi.org/10.1021/acs.inorgchem.6c02837
Inorg. Chem. 2026, 65, 19417−19428

Despite this qualitative agreement, some quantitative discrepancies persist. The simulated molar absorptivity of the aqua ion is approximately 30% lower than the experimental value (550 M^{-1} cm^{-1}). The computed bands are also broader than the experimental ones, an effect likely coming from the sampling procedure and the Gaussian Mixture Model (GMM) methodology, although the GMM approach is intended to minimize the arbitrary assignment of half-widths. The theoretical bands are more closely spaced than those observed in the experimental evolution, suggesting that the current model underestimates relative energy differences between successive species.

The calculated intensity of the tetrachloride complex, $[PuO_2Cl_4]^{2-}$, is negligible compared to the lower-order species. This reduced oscillator strength suggests a potential quenching of the transition probabilities, possibly due to the increased symmetry of the tetrachloride coordination environment or an insufficient description of the transition dipoles at this level of theory. This low computed intensity complicates a direct assignment of the experimental features at 16 M Cl^- to the tetrachloride species. However, at such extreme salinity, the presence of water in the first coordination shell is chemically improbable, and existing Raman experimental evidence is consistent with the formation of the tetrachloride complex. The theoretical methodology accurately tracks the energetic evolution across the full series, even though the precise spectral characterization of the highest-order complexes remains limited by the current model.

CONCLUSIONS

In the $[PuO_2(H_2O)_mCl_n]^{2-n}$ series, the plutonyl core is highly sensitive to the equatorial ligand field. Progressive replacement of water by chloride elongates the Pu−O_{yl} bond through increased equatorial electron donation from the anionic ligands. The most pronounced structural reorganization is the transition from the pentacoordinated equatorial plane (D_{5h}) to the tetracoordinated geometry (D_{4h}) in the $[PuO_2Cl_4]^{2-}$ complex, which relieves steric repulsion and provides a molecular basis for the vibrational signatures observed for the Raman B_{2g} mode at high salinity.

The MP2-Wigner sampled geometries reproduce the L_{III}-edge EXAFS and XANES spectra with high fidelity. In the EXAFS spectra, the interference pattern between Pu−O_{yl} and equatorial Pu−OH_2 or Pu−Cl paths in the k region between 7 $Å^{-1}$ and 8 $Å^{-1}$, constitutes a key structural fingerprint for chloride coordination. Consistent with the experimental features, XANES calculations confirm that the *trans*-dioxo geometry and Pu(VI) oxidation state are preserved even when the equatorial shell undergoes significant electronic perturbation.

For the $5f^2$ electronic manifold, both NEVPT2 and CASPT2 effectively recover the relative energy spacing of the excited states from the $[PuO_2(H_2O)_5]^{2+}$-optimized structure. Both methods exhibit a systematic blue shift, partially corrected with the use of a scaling factor. NEVPT2 was adopted for its parameter-free formulation and the higher computational efficiency with the cc-pVQZ-X2C basis, enabling its application to the full Wigner ensemble.

The UV−vis spectrum shows high sensitivity to configurational sampling. Classical MD trajectories based on B3LYP parametrized force fields introduced excessive inhomogeneous broadening, while Wigner sampling successfully reproduced the sharp feature of the experimental band F. The difference between the two approaches makes the UV−vis spectrum a direct diagnostic of the quality of the structural ensemble.

The methodology successfully captures the experimental red-shift trend across the full substitution series, from 12,045 cm^{-1} in the aqua ion to the lower energy bands of the chloro complexes. The transition intensities for $[PuO_2Cl_4]^{2-}$ are underestimated, resulting in a band at approximately 11,600 cm^{-1} of almost negligible intensity. Preliminary analysis shows that the intensity of the transition is stronger for the structures with more distorted geometries of the tetrachloro complex. However, the average of the samples cancels out these contributions. This means that adding anharmonic corrections to the Wigner sampling could help improve the structural fluctuations of plutonyl complexes, especially those with high symmetry. The computed energetic shifts allow for the individual contributions of each complex to be isolated, even for species that coexist in equilibrium without isolated experimental references.

ASSOCIATED CONTENT

Data Availability Statement

The data set supporting the findings of this work is available in 10.12795/11441/186210.

Supporting Information

The Supporting Information is available free of charge at https://pubs.acs.org/doi/10.1021/acs.inorgchem.6c02837.

ORCA and FEFF input files; structural models for the aqua ion and the aqua−chloro complexes; comparison of experimental and theoretical EXAFS spectra for $[PuO_2(H_2O)_5]^{2+}$; EXAFS SS contributions for $[PuO_2(H_2O)_5]^{2+}$; experimental[21] Pu M4-edge XANES spectrum of PuO_2^{2+} in aqueous solution and 6 M hydrochloric acid; theoretical Pu M4-edge XANES spectrum of $[PuO_2(H_2O)_5]^{2+}$ and $[PuO_2(H_2O)_2Cl_3]^-$; evolution of experimental UV−vis spectra shown; comparison of UV−vis for $[PuO_2(H_2O)_5]^{2+}$ obtained from MD and Wigner sampling; Pu−O and O−H distance distribution; and contribution of isomers of $[PuO_2(H_2O)_3Cl_2]^{2+}$ and $[PuO_2(H_2O)_2Cl_3]^-$ to the UV−vis (PDF)

AUTHOR INFORMATION

Corresponding Author

Enrique Sánchez Marcos − *Department of Physical Chemistry, University of Seville, 41012 Seville, Spain;* orcid.org/0000-0002-8367-9105; Email: sanchez@us.es

Authors

Gema Raposo-Hernández − *Department of Physical Chemistry, University of Seville, 41012 Seville, Spain;* orcid.org/0000-0001-7461-664X

Rafael R. Pappalardo − *Department of Physical Chemistry, University of Seville, 41012 Seville, Spain;* orcid.org/0000-0003-3751-2395

Andrea Melchior − *Dipartimento Politecnico di Ingegneria e Architettura, Laboratorio di Tecnologie Chimiche, Università di Udine, 33100 Udine, Italy;* orcid.org/0000-0002-5265-1396

Complete contact information is available at: https://pubs.acs.org/10.1021/acs.inorgchem.6c02837

Notes

The authors declare no competing financial interest.

■ ACKNOWLEDGMENTS

GRH acknowledges support through a Ph.D. grant (PIF, VI PPIT-US) from the University of Seville and the funded research stay at the University of Udine.

■ REFERENCES

(1) Dasgupta, S.; Peng, X.; Chen, S.; Li, J.; Du, M.; Xu, H.; Ta, K.; Zhou, Y.-H.; Zhong, G. Toxic Anthropogenic Pollutants Reach the Deepest Ocean on Earth. *Geochem. Perspect. Lett.* **2018**, *7*, 22−26.
(2) Zitoun, R.; Marcinek, S.; Hatje, V.; Sander, S. G.; Völker, C.; Sarin, M.; Omanović, D. Climate Change Driven Effects on Transport, Fate and Biogeochemistry of Trace Element Contaminants in Coastal Marine Ecosystems. *Commun. Earth Environ.* **2024**, *5*, 560.
(3) Hatje, V.; Sarin, M.; Sander, S. G.; Omanović, D.; Ramachandran, P.; Völker, C.; Barra, R. O.; Tagliabue, A. Emergent Interactive Effects of Climate Change and Contaminants in Coastal and Ocean Ecosystems. *Front. Mar. Sci.* **2022**, *9*, 936109.
(4) Thiagarajan, C.; Devarajan, Y. The Urgent Challenge of Ocean Pollution: Impacts on Marine Biodiversity and Human Health. *Reg. Stud. Mar. Sci.* **2025**, *81*, 103995.
(5) *Energy Statistics Data Browser*. https://www.iea.org/data-and-statistics/data-tools/energy-statistics-data-browser. (accessed Dec 16, 2025).
(6) Runde, W.; Neu, M. P.; Conradson, S. D.; Clark, D. L.; Palmer, P. D.; Reilly, S. D.; Scott, B. L.; Tait, C. D. Spectroscopic Investigation of Actinide Speciation in Concentrated Chloride Solution. *MRS Proc.* **1996**, *465*, 693.
(7) Belkessa, N.; Burie, B.; Creff, G.; Jeanson, A.; Rammal, M.; Solari, P.-L.; Prieur, D.; Harrington, M. J.; Den Auwer, C. Uranium and Neptunium Accumulation by the Byssus of *MytilusGalloprovincialis*. *Eur. J. Inorg. Chem.* **2026**, *29*, No. e202500438.
(8) *Toxicological Profile for Plutonium*; Agency for Toxic Substances and Disease Registry (US): Atlanta, 2010.
(9) Harley, J. H. Plutonium in the Environment—A Review. *J. Radiat. Res.* **1980**, *21*, 83−104.
(10) Livingston, H. D.; Povinec, P. P. A Millennium Perspective on the Contribution of Global Fallout Radionuclides to Ocean Science. *Health Phys.* **2002**, *82*, 656.
(11) Zheng, J.; Tagami, K.; Uchida, S. Release of Plutonium Isotopes into the Environment from the Fukushima Daiichi Nuclear Power Plant Accident: What Is Known and What Needs to Be Known. *Environ. Sci. Technol.* **2013**, *47*, 9584−9595.
(12) Kurihara, E.; Takehara, M.; Suetake, M.; Ikehara, R.; Komiya, T.; Morooka, K.; Takami, R.; Yamasaki, S.; Ohnuki, T.; Horie, K.; Takehara, M.; Law, G. T. W.; Bower, W.; Mosselmans, J. F. W.; Warnicke, P.; Grambow, B.; Ewing, R. C.; Utsunomiya, S. Particulate Plutonium Released from the Fukushima Daiichi Meltdowns. *Sci. Total Environ.* **2020**, *743*, 140539.
(13) Millero, F. J.; Woosley, R.; DiTrolio, B.; Waters, J. Effect of Ocean Acidification on the Speciation of Metals in Seawater. *Oceanogr.* **2009**, *22*, 72−85.
(14) Bardin, N.; Rubini, P.; Madie, C. Hydration of Actinyl(VI), MO_{2aq}^{2+} (M = U, Np, Pu). An NMR Study. *Radiochim. Acta* **1998**, *83*, 189−194.
(15) Clark, D. L.; Hecker, i. S.; Jarvinen, G. D.; Neu, M. P. *The Chemistry of the Actinide and Transactinide Elements*; Springer: Netherlands, 2006; Vol. 2, pp 813−1264.
(16) Mckibben, J. M. Chemistry of the Purex Process. *Radiochim. Acta* **1984**, *36*, 3−16.
(17) Su, J.; Dau, P. D.; Qiu, Y.-H.; Liu, H.-T.; Xu, C.-F.; Huang, D.-L.; Wang, L.-S.; Li, J. Probing the Electronic Structure and Chemical Bonding in Tricoordinate Uranyl Complexes $UO_2X_3^-$ (X = F, Cl, Br, I): Competition between Coulomb Repulsion and U−X Bonding. *Inorg. Chem.* **2013**, *52*, 6617−6626.
(18) Vallet, V.; Wahlgren, U.; Grenthe, I. Probing the Nature of Chemical Bonding in Uranyl(VI) Complexes with Quantum Chemical Methods. *J. Phys. Chem. A* **2012**, *116*, 12373−12380.
(19) Wilson, R. E.; Skanthakumar, S.; Cahill, C. L.; Soderholm, L. Structural Studies Coupling X-ray Diffraction and High-Energy X-ray Scattering in the UO_2^{2+}−HBr_{aq} System. *Inorg. Chem.* **2011**, *50*, 10748−10754.
(20) Crawford, M.-J.; Mayer, P. S. Structural and Computational Investigations of $UO_2I_4^{2-}$: A Structurally Characterized U(VI)-I Anion. *Inorg. Chem.* **2005**, *44*, 5547−5549.
(21) Neill, T. S.; Ramanantoanina, H.; Palina, N.; Prüßmann, T.; Rothe, J.; Gaona, X.; Fellhauer, D.; Schild, D.; Wansorra, C.; Hauschild, D.; Steininger, R.; Schacherl, B.; Heske, C.; Weinhardt, L.; Walter, O.; Weigend, F.; Vitova, T. The Role of Halides in the Bonding and Electronic Structure of Actinyl(VI) Halides-Energy Match Driven Stability. *J. Am. Chem. Soc.* **2025**, *147*, 35401−35412.
(22) Runde, W.; Reilly, S. D.; Neu, M. P. Spectroscopic Investigation of the Formation of PuO_2Cl^+ and PuO_2Cl_2 in NaCl Solutions and Application for Natural Brine Solutions. *Geochim. Cosmochim. Acta* **1999**, *63*, 3443−3449.
(23) Maher, K.; Bargar, J. R.; Brown, G. E. J. Environmental Speciation of Actinides. *Inorg. Chem.* **2013**, *52*, 3510−3532.
(24) Allen, P. G.; Bucher, J. J.; Shuh, D. K.; Edelstein, N. M.; Reich, T. Investigation of Aquo and Chloro Complexes of UO_2^{2+}, NpO_2^+, Np^{4+}, and Pu^{3+} by X-ray Absorption Fine Structure Spectroscopy. *Inorg. Chem.* **1997**, *36*, 4676−4683.
(25) Neuefeind, J.; Soderholm, L.; Skanthakumar, S. Experimental Coordination Environment of Uranyl(VI) in Aqueous Solution. *J. Phys. Chem. A* **2004**, *108*, 2733−2739.
(26) Pérez-Conesa, S.; Martínez, J. M.; Pappalardo, R. R.; Sánchez Marcos, E. Combining EXAFS and Computer Simulations to Refine the Structural Description of Actinyls in Water. *Molecules* **2020**, *25*, 5250.
(27) Soderholm, L.; Skanthakumar, S.; Neuefeind, J. Determination of Actinide Speciation in Solution Using High-Energy X-ray Scattering. *Anal. Bioanal. Chem.* **2005**, *383*, 48−55.
(28) Conradson, S. D. Application of X-Ray Absorption Fine Structure Spectroscopy to Materials and Environmental Science. *Appl. Spectrosc.* **1998**, *52*, 252A−279A.
(29) Aaberg, M.; Ferri, D.; Glaser, J.; Grenthe, I. Structure of the Hydrated Dioxouranium(VI) Ion in Aqueous Solution. An X-ray Diffraction and Proton NMR Study. *Inorg. Chem.* **1983**, *22*, 3986−3989.
(30) Odoh, S. O.; Schreckenbach, G. Theoretical Study of the Structural Properties of Plutonium(IV) and (VI) Complexes. *J. Phys. Chem. A* **2011**, *115*, 14110−14119.
(31) Conradson, S. D.; Abney, K. D.; Begg, B. D.; Brady, E. D.; Clark, D. L.; den Auwer, C.; Ding, M.; Dorhout, P. K.; Espinosa-Faller, F. J.; Gordon, P. L.; Haire, R. G.; Hess, N. J.; Hess, R. F.; Keogh, D. W.; Lander, G. H.; Lupinetti, A. J.; Morales, L. A.; Neu, M. P.; Palmer, P. D.; Paviet-Hartmann, P.; Reilly, S. D.; Runde, W. H.; Tait, C. D.; Veirs, D. K.; Wastin, F. Higher Order Speciation Effects on Plutonium L_3 X-ray Absorption Near Edge Spectra. *Inorg. Chem.* **2004**, *43*, 116−131.
(32) Gaunt, A. J.; May, I.; Neu, M. P.; Reilly, S. D.; Scott, B. L. Structural and Spectroscopic Characterization of Plutonyl(VI) Nitrate under Acidic Conditions. *Inorg. Chem.* **2011**, *50*, 4244−4246.
(33) Prieur, D.; Amidani, L.; Bazarkina, E. F.; Hennig, C.; Lawrence Bright, E.; Rossberg, A.; Silva, C. L.; Kvashnina, K. O. Frontiers of Synchrotron Methods for Actinide Science. *Chem. Methods* **2025**, *5*, No. e202400073.
(34) Austin, J. P.; Sundararajan, M.; Vincent, M. A.; Hillier, I. H. The Geometric Structures, Vibrational Frequencies and Redox Properties of the Actinyl Coordination Complexes ($[AnO_2(L)_n]^m$; An = U, Pu, Np; L = H_2O, Cl^-, CO_3^{2-}, $CH_3CO_2^-$, OH^-) in Aqueous Solution, Studied by Density Functional Theory Methods. *Dalton Trans.* **2009**, 5902−5909.

(35) Du, J.; Sun, X.; Jiang, G. Exploring the Interaction Natures in Plutonyl (VI) Complexes with Topological Analyses of Electron Density. *Int. J. Mol. Sci.* **2016**, *17*, 414.
(36) Boguslawski, K.; Réal, F.; Tecmer, P.; Duperrouzel, C.; Gomes, A. S. P.; Legeza, O.; Ayers, P. W.; Vallet, V. On the Multi-Reference Nature of Plutonium Oxides: PuO_2^{2+}, PuO_2, PuO_3 and $PuO_2(OH)_2$. *Phys. Chem. Chem. Phys.* **2017**, *19*, 4317−4329.
(37) Adeyiga, O.; Suleiman, O.; Dandu, N. K.; Odoh, S. O. Ground-State Actinide Chemistry with Scalar-Relativistic Multiconfiguration Pair-Density Functional Theory. *J. Chem. Phys.* **2019**, *151*, 134102.
(38) Matsika, S.; Pitzer, R. M.; Reed, D. T. Intensities in the Spectra of Actinyl Ions. *J. Phys. Chem. A* **2000**, *104*, 11983−11992.
(39) Danilo, C.; Vallet, V.; Flament, J.-P.; Wahlgren, U. Effects of the First Hydration Sphere and the Bulk Solvent on the Spectra of the f^2 Isoelectronic Actinide Compounds: U^{4+}, NpO_2^{+}, and PuO_2^{2+}. *Phys. Chem. Chem. Phys.* **2010**, *12*, 1116−1130.
(40) Raposo-Hernández, G.; Pappalardo, R. R.; Réal, F.; Vallet, V.; Sánchez Marcos, E. Toward a Realistic Theoretical Electronic Spectra of Metal Aqua Ions in Solution: The Case of $Ce(H_2O)_n^{3+}$ Using Statistical Methods and Quantum Chemistry Calculations. *J. Chem. Phys.* **2024**, *161*, 144109.
(41) Raposo-Hernández, G.; Pappalardo, R. R.; Réal, F.; Vallet, V.; Sánchez Marcos, E. U^{4+} Speciation in Acidic Aqueous Solution: Insights from UV−Vis, EXAFS, XANES, and Quantum-Statistical Simulations. *Inorg. Chem.* **2025**, *64*, 15321−15331.
(42) Wernbacher, A. M.; González, L. The Importance of Finite Temperature and Vibrational Sampling in the Absorption Spectrum of a Nitro-Functionalized Ru(II) Water Oxidation Catalyst. *Phys. Chem. Chem. Phys.* **2021**, *23*, 17724−17733.
(43) Mai, S.; Gattuso, H.; Fumanal, M.; Muñoz-Losa, A.; Monari, A.; Daniel, C.; González, L. Excited-States of a Rhenium Carbonyl Diimine Complex: Solvation Models, Spin−Orbit Coupling, and Vibrational Sampling Effects. *Phys. Chem. Chem. Phys.* **2017**, *19*, 27240−27250.
(44) Carmona-García, J.; Saiz-Lopez, A.; Mahajan, A. S.; Wang, F.; Borrego-Sánchez, A.; Acuña, A. U.; Cuevas, C. A.; Dávalos, J. Z.; Feinberg, A.; Spolaor, A.; Ruiz-López, M. F.; Francisco, J. S.; Roca-Sanjuán, D. Photoreduction of Mercuric Bromides in Polar Ice. *Proc. Natl. Acad. Sci. U. S. A.* **2025**, *122*, No. e2422885122.
(45) Cao, X.; Dolg, M. Segmented Contraction Scheme for Small-Core Actinide Pseudopotential Basis Sets. *J. Mol. Struct.: THEOCHEM* **2004**, *673*, 203−209.
(46) Küchle, W.; Dolg, M.; Stoll, H.; Preuss, H. Energy-adjusted Pseudopotentials for the Actinides. Parameter Sets and Test Calculations for Thorium and Thorium Monoxide. *J. Chem. Phys.* **1994**, *100*, 7535−7542.
(47) Cao, X.; Dolg, M.; Stoll, H. Valence Basis Sets for Relativistic Energy-Consistent Small-Core Actinide Pseudopotentials. *J. Chem. Phys.* **2003**, *118*, 487−496.
(48) Dunning, T. H., Jr Gaussian Basis Sets for Use in Correlated Molecular Calculations. I. The Atoms Boron through Neon and Hydrogen. *J. Chem. Phys.* **1989**, *90*, 1007−1023.
(49) Woon, D. E.; Dunning, T. H., Jr Gaussian Basis Sets for Use in Correlated Molecular Calculations. III. The Atoms Aluminum through Argon. *J. Chem. Phys.* **1993**, *98*, 1358−1371.
(50) Barone, V.; Cossi, M. Quantum Calculation of Molecular Energies and Energy Gradients in Solution by a Conductor Solvent Model. *J. Phys. Chem. A* **1998**, *102*, 1995−2001.
(51) Siegbahn, P.; Heiberg, A.; Roos, B.; Levy, B. A Comparison of the Super-CI and the Newton-Raphson Scheme in the Complete Active Space SCF Method. *Phys. Scr.* **1980**, *21*, 323.
(52) Roos, B. O.; Taylor, P. R.; Siegbahn, P. E. M. A Complete Active Space SCF Method (CASSCF) Using a Density Matrix Formulated Super-CI Approach. *Chem. Phys.* **1980**, *48*, 157−173.
(53) Siegbahn, P. E. M.; Almlöf, J.; Heiberg, A.; Roos, B. O. The Complete Active Space SCF (CASSCF) Method in a Newton−Raphson Formulation with Application to the HNO Molecule. *J. Chem. Phys.* **1981**, *74*, 2384−2396.
(54) Angeli, C.; Cimiraglia, R.; Evangelisti, S.; Leininger, T.; Malrieu, J.-P. Introduction of N-Electron Valence States for Multireference Perturbation Theory. *J. Chem. Phys.* **2001**, *114*, 10252−10264.
(55) Angeli, C.; Cimiraglia, R.; Malrieu, J.-P. *N*-Electron Valence State Perturbation Theory: A Fast Implementation of the Strongly Contracted Variant. *Chem. Phys. Lett.* **2001**, *350*, 297−305.
(56) Angeli, C.; Cimiraglia, R.; Malrieu, J.-P. N-Electron Valence State Perturbation Theory: A Spinless Formulation and an Efficient Implementation of the Strongly Contracted and of the Partially Contracted Variants. *J. Chem. Phys.* **2002**, *117*, 9138−9153.
(57) Andersson, K.; Malmqvist, P. A.; Roos, B. O.; Sadlej, A. J.; Wolinski, K. Second-Order Perturbation Theory with a CASSCF Reference Function. *J. Phys. Chem.* **1990**, *94*, 5483−5488.
(58) Andersson, K.; Malmqvist, P.-Å.; Roos, B. O. Second-order Perturbation Theory with a Complete Active Space Self-consistent Field Reference Function. *J. Chem. Phys.* **1992**, *96*, 1218−1226.
(59) Finley, J.; Malmqvist, P.-Å.; Roos, B. O.; Serrano-Andrés, L. The Multi-State CASPT2Method. *Chem. Phys. Lett.* **1998**, *288*, 299−306.
(60) Ghigo, G.; Roos, B. O.; Malmqvist, P.-Å. A Modified Definition of the Zeroth-Order Hamiltonian in Multiconfigurational Perturbation Theory (CASPT2). *Chem. Phys. Lett.* **2004**, *396*, 142−149.
(61) Leszczyk, A.; Tecmer, P.; Boguslawski, K. *Transition Metals in Coordination Environments: Computational Chemistry and Catalysis Viewpoints*; Broclawik, E., Borowski, T., Radoń, M., Eds.; Springer International Publishing: Cham, 2019; pp 121−160..
(62) Lu, L.; Hu, H.; Jenkins, A. J.; Li, X. Exact-Two-Component Relativistic Multireference Second-Order Perturbation Theory. *J. Chem. Theory Comput.* **2022**, *18*, 2983−2992.
(63) Sharma, P.; Jenkins, A. J.; Scalmani, G.; Frisch, M. J.; Truhlar, D. G.; Gagliardi, L.; Li, X. Exact-Two-Component Multiconfiguration Pair-Density Functional Theory. *J. Chem. Theory Comput.* **2022**, *18*, 2947−2954.
(64) Hu, H.; Jenkins, A. J.; Liu, H.; Kasper, J. M.; Frisch, M. J.; Li, X. Relativistic Two-Component Multireference Configuration Interaction Method with Tunable Correlation Space. *J. Chem. Theory Comput.* **2020**, *16*, 2975−2984.
(65) Knecht, S.; Jensen, H. J. A.; Saue, T. Relativistic Quantum Chemical Calculations Show That the Uranium Molecule U2 Has a Quadruple Bond. *Nature Chem.* **2019**, *11*, 40−44.
(66) Pollak, P.; Weigend, F. Segmented Contracted Error-Consistent Basis Sets of Double- and Triple-ζ Valence Quality for One- and Two-Component Relativistic All-Electron Calculations. *J. Chem. Theory Comput.* **2017**, *13*, 3696−3705.
(67) Franzke, Y. J.; Treß, R.; Pazdera, T. M.; Weigend, F. Error-Consistent Segmented Contracted All-Electron Relativistic Basis Sets of Double- and Triple-Zeta Quality for NMR Shielding Constants. *Phys. Chem. Chem. Phys.* **2019**, *21*, 16658−16664.
(68) Feng, R.; Peterson, K. A. Correlation Consistent Basis Sets for Actinides. II. The Atoms Ac and Np−Lr. *J. Chem. Phys.* **2017**, *147*, 084108.
(69) Feng, R.; Duignan, T. J.; Autschbach, J. Electron−Nucleus Hyperfine Coupling Calculated from Restricted Active Space Wavefunctions and an Exact Two-Component Hamiltonian. *J. Chem. Theory Comput.* **2021**, *17*, 255−268.
(70) Mussard, B.; Sharma, S. One-Step Treatment of Spin−Orbit Coupling and Electron Correlation in Large Active Spaces. *J. Chem. Theory Comput.* **2018**, *14*, 154−165.
(71) Ganyushin, D.; Neese, F. First-Principles Calculations of Zero-Field Splitting Parameters. *J. Chem. Phys.* **2006**, *125*, 024103.
(72) Neese, F. The ORCA Program System. *Wiley Interdiscip. Rev. Comput. Mol. Sci.* **2012**, *2*, 73−78.
(73) Neese, F. Software Update: The ORCA Program System—Version 6.0. *Wiley Interdiscip. Rev. Comput. Mol. Sci.* **2025**, *15*, No. e70019.
(74) Pérez-Conesa, S.; Torrico, F.; Martínez, J. M.; Pappalardo, R. R.; Sánchez Marcos, E. A Hydrated Ion Model of $[UO_2]^{2+}$ in Water:

https://doi.org/10.1021/acs.inorgchem.6c02837
Inorg. Chem. 2026, 65, 19417−19428

Structure, Dynamics, and Spectroscopy from Classical Molecular Dynamics. *J. Chem. Phys.* **2016**, *145*, 224502.
(75) Pérez-Conesa, S.; Martínez, J. M.; Pappalardo, R. R.; Sánchez Marcos, E. Extracting the Americyl Hydration from an Americium Cationic Mixture in Solution: A Combined X-ray Absorption Spectroscopy and Molecular Dynamics Study. *Inorg. Chem.* **2018**, *57*, 8089−8097.
(76) Pérez-Conesa, S.; Torrico, F.; Martínez, J. M.; Pappalardo, R. R.; Sánchez Marcos, E. A General Study of Actinyl Hydration by Molecular Dynamics Simulations Using Ab Initio Force Fields. *J. Chem. Phys.* **2019**, *150*, 104504.
(77) Crespo-Otero, R.; Barbatti, M. *Marco Antonio Chaer Nascimento: A Festschrift from Theoretical Chemistry Accounts*; Ornellas, F. R., João Ramos, M., Eds.; Springer: Berlin, Heidelberg, 2014; pp 89−102.
(78) Barbatti, M.; Aquino, A. J. A.; Lischka, H. The UV Absorption of Nucleobases: Semi-classical Ab Initio Spectra Simulations. *Phys. Chem. Chem. Phys.* **2010**, *12*, 4959−4967.
(79) Saiz-Lopez, A.; Sitkiewicz, S. P.; Roca-Sanjuán, D.; Oliva-Enrich, J. M.; Dávalos, J. Z.; Notario, R.; Jiskra, M.; Xu, Y.; Wang, F.; Thackray, C. P.; Sunderland, E. M.; Jacob, D. J.; Travnikov, O.; Cuevas, C. A.; Acuña, A. U.; Rivero, D.; Plane, J. M. C.; Kinnison, D. E.; Sonke, J. E. Photoreduction of Gaseous Oxidized Mercury Changes Global Atmospheric Mercury Speciation, Transport and Deposition. *Nat. Commun.* **2018**, *9*, 4796.
(80) Wigner, E. On the Quantum Correction For Thermodynamic Equilibrium. *Phys. Rev.* **1932**, *40*, 749−759.
(81) Mai, S.; Bachmair, B.; Gagliardi, L.; Gallmetzer, H. G.; Grünewald, L.; Hennefarth, M.; Machholdt Høyer, N.; Korsaye, F. A.; Mausenberger, S.; Oppel, M.; Piteša, T.; Polonius, S.; Sangiogo Gil, E.; Shu, Y.; Singer, N. K.; Tiefenbacher, M. X.; Truhlar, D.; Vörös, D.; Zhang, L.; Gonzalez, L. *SHARC4.0: Surface Hopping Including Arbitrary Couplings − Program Package for Non-adiabatic Dynamics*; Zenodo, 2025.
(82) Prlj, A.; Hollas, D.; Curchod, B. F. E. Deciphering the Influence of Ground-State Distributions on the Calculation of Photolysis Observables. *J. Phys. Chem. A* **2023**, *127*, 7400−7409.
(83) Favero, L.; Granucci, G.; Persico, M. Dynamics of Acetone Photodissociation: A Surface Hopping Study. *Phys. Chem. Chem. Phys.* **2013**, *15*, 20651−20661.
(84) Merkling, P. J.; Muñoz-Páez, A.; Sánchez Marcos, E. Exploring the Capabilities of X-ray Absorption Spectroscopy for Determining the Structure of Electrolyte Solutions: Computed Spectra for Cr^{3+} or Rh^{3+} in Water Based on Molecular Dynamics. *J. Am. Chem. Soc.* **2002**, *124*, 10911−10920.
(85) Carrera, F.; Torrico, F.; Richens, D. T.; Muñoz-Páez, A.; Martínez, J. M.; Pappalardo, R. R.; Sánchez Marcos, E. Combined Experimental and Theoretical Approach to the Study of Structure and Dynamics of the Most Inert Aqua Ion $[Ir(H_2O)_6]^{3+}$ in Aqueous Solution. *J. Phys. Chem. B* **2007**, *111*, 8223−8233.
(86) Raposo-Hernández, G.; Martínez, J. M.; Pappalardo, R. R.; Den Auwer, C.; Sánchez Marcos, E. A Coupled EXAFS−Molecular Dynamics Study on PuO_2^+ and NpO_2^+ Hydration: The Importance of Electron Correlation in Force-Field Building. *Inorg. Chem.* **2022**, *61*, 8703−8714.
(87) Kas, J. J.; Vila, F. D.; Pemmaraju, C. D.; Tan, T. S.; Rehr, J. J. Advanced Calculations of X-ray Spectroscopies with FEFF10 and Corvus. *J. Synchrotron Radiat.* **2021**, *28*, 1801−1810.
(88) Rehr, J. J.; Kas, J. J.; Vila, F. D.; Prange, M. P.; Jorissen, K. Parameter-Free Calculations of X-ray Spectra with FEFF9. *Phys. Chem. Chem. Phys.* **2010**, *12*, 5503−5513.
(89) Cerdán, L.; Roca-Sanjuán, D. Reconstruction of Nuclear Ensemble Approach Electronic Spectra Using Probabilistic Machine Learning. *J. Chem. Theory Comput.* **2022**, *18*, 3052−3064.
(90) Kumar, N.; Seminario, J. M. Solvation of Actinide Salts in Water Using a Polarizable Continuum Model. *J. Phys. Chem. A* **2015**, *119*, 689−703.
(91) Reich, T.; Geipel, G.; Funke, H.; Hennig, C.; Roßberg, A.; Bernhard, G. *XANES and EXAFS Measurements of Plutonium Hydrates*; Project-Group ESRF-Beamline (ROBl-eRG), 2001.
(92) Ayala, R.; Martínez, J. M.; Pappalardo, R. R.; Muñoz Páez, A.; Sánchez Marcos, E. General Quantum-Mechanical Study on the Hydrolysis Equilibria for a Tetravalent Aquaion: The Extreme Case of the Po(IV) in Water. *J. Phys. Chem. B* **2009**, *113*, 487−496.
(93) Holovko, M.; Druchok, M.; Bryk, T. A Molecular Dynamics Modelling of Cation Hydrolysis Effects. *J. Electroanal. Chem.* **2005**, *582*, 50−56.
(94) Fillaux, C.; Berthet, J.-C.; Conradson, S. D.; Guilbaud, P.; Guillaumont, D.; Hennig, C.; Moisy, P.; Roques, J.; Simoni, E.; Shuh, D. K.; Tyliszczak, T.; Castro-Rodriguez, I.; Den Auwer, C. Combining Theoretical Chemistry and XANES Multi-Edge Experiments to Probe Actinide Valence States. *C. R. Chim.* **2007**, *10*, 859−871.
(95) Edelstein, N. M. Revisiting the Optical Spectrum of the Plutonyl Ion $(PuO_2)^{2+}$ in 1 M $HClO_4$. *J. Phys. Chem. A* **2025**, *129*, 50−57.
(96) Acher, E.; Masella, M.; Vallet, V.; Réal, F. Properties of the Tetravalent Actinide Series in Aqueous Phase from a Microscopic Simulation Self-Consistent Engine. *Phys. Chem. Chem. Phys.* **2020**, *22*, 2343−2350.
(97) Cohen, D. The Absorption Spectra of Plutonium Ions in Perchloric Acid Solutions. *J. Inorg. Nucl. Chem.* **1961**, *18*, 211−218.
(98) Lee, M. H.; Park, Y. J.; Kim, W. H. Absorption Spectroscopic Properties for Pu(III, IV and VI) in Nitric and Hydrochloric Acid Media. *J. Radioanal. Nucl. Chem.* **2007**, *273*, 375−382.

https://doi.org/10.1021/acs.inorgchem.6c02837
Inorg. Chem. 2026, 65, 19417−19428